

ISSN: 0256-307X

# 中国物理快报

# Chinese Physics Letters

Volume 32 Number 9 September 2015

A Series Journal of the Chinese Physical Society  
Distributed by IOP Publishing

Online: <http://iopscience.iop.org/0256-307X>  
<http://cpl.iphy.ac.cn>

CHINESE PHYSICAL SOCIETY  
**IOP** Publishing

JUST FOR AUTHORS  
— CHINESE PHYSICS LETTERS

# First Evaluation and Frequency Measurement of the Strontium Optical Lattice Clock at NIM \*

LIN Yi-Ge(林弋戈)<sup>1\*\*</sup>, WANG Qiang(王强)<sup>1,2</sup>, LI Ye(李焯)<sup>1,2</sup>, MENG Fei(孟飞)<sup>1</sup>, LIN Bai-Ke(林百科)<sup>1,2</sup>, ZANG Er-Jun(臧二军)<sup>1</sup>, SUN Zhen(孙震)<sup>1</sup>, FANG Fang(房芳)<sup>1</sup>, LI Tian-Chu(李天初)<sup>1</sup>, FANG Zhan-Jun(方占军)<sup>1</sup>

<sup>1</sup>Division of Time and Frequency, National Institute of Metrology (NIM), Beijing 100013

<sup>2</sup>Department of Precision Instrument, Tsinghua University, Beijing 100084

(Received 31 July 2015)

An optical lattice clock based on  $^{87}\text{Sr}$  is built at National Institute of Metrology (NIM) of China. The systematic frequency shifts of the clock are evaluated with a total uncertainty of  $2.3 \times 10^{-16}$ . To measure its absolute frequency with respect to NIM's cesium fountain clock NIM5, the frequency of a flywheel H-maser of NIM5 is transferred to the Sr laboratory through a 50-km-long fiber. A fiber optical frequency comb, phase-locked to the reference frequency of this H-maser, is used for the optical frequency measurement. The absolute frequency of this Sr clock is measured to be  $429228004229873.7(1.4)$  Hz.

PACS: 06.30.Ft, 42.62.Fi, 32.70.Jz, 37.10.Jk, 42.62.Eh

DOI: 10.1088/0256-307X/32/9/090601

Optical clocks have shown the ability to be extremely precise. Some of these clocks have reported an accuracy at the 18th digit,<sup>[1–4]</sup> which could potentially be used to explore the possible time variation of some fundamental physical constants such as the fine-structure constant ( $\alpha$ ).<sup>[5]</sup> Although the accuracy of optical clocks has surpassed the best cesium fountain clocks, their absolute frequency still needs to be traced to the Cs primary frequency standard under the current international system of units (SI). To know the absolute frequency of an optical clock more precisely, it is always better to have more laboratories to carry out the frequency measurements independently. Here we present the systematic uncertainty evaluation and frequency measurement of the optical lattice clock based on  $^{87}\text{Sr}$  at NIM.

We will give the details of the evaluation and frequency measurement, more information of the clock and related experiments can be found in Refs. [6–9]. The simplified level scheme of  $^{87}\text{Sr}$  is shown in Fig. 1(a). The first-stage magneto-optical trap (MOT) of  $^{87}\text{Sr}$  is operated on the  $^1S_0$ – $^1P_1$  transition at 461 nm with a natural linewidth of 32 MHz.<sup>[6]</sup> Two re-pumping lasers at 679 nm and 707 nm are used to improve the loading efficiency, respectively. The second-stage MOT cools the atoms down to as low as  $3 \mu\text{K}$  utilizing the  $^1S_0$ – $^3P_1$  transition at 689 nm with a natural linewidth of 7.5 kHz.<sup>[7]</sup> During the cooling process, the 813 nm lattice laser is overlapped with the atom cloud all the time. The lattice laser is a commercial Ti:sapphire laser (Coherent MBR110 pumped by a Verdi-V10). The 1D optical lattice is horizontally oriented.<sup>[7]</sup> The lattice beam waist is  $\sim 42 \mu\text{m}$  and the trap depth is  $29 \mu\text{K}$ . The 698 nm laser is locked to a high finesse reference cavity with the PDH method to

narrow its linewidth.<sup>[8]</sup> An AOM driven by a direct-digital synthesizer (DDS) is used to compensate for the drift of the cavity.

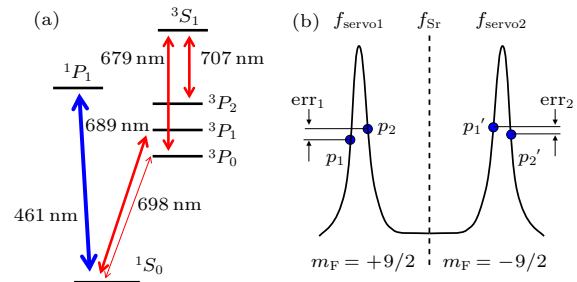


**Fig. 1.** The schematic diagram of the experiment. (a) Simplified level scheme of  $^{87}\text{Sr}$ . (b) The clock transition locking method. Two servos lock the laser frequency time-multiplexed to the two transitions ( $m_F = +9/2$  and  $m_F = -9/2$ ) by using the differential transition probabilities ( $p_1 - p_2$  or  $p'_1 - p'_2$ ) as the error signal. The center frequency of these two servos gives the frequency of the Sr clock.

To find the  $^1S_0$ – $^3P_0$  clock transition, the clock laser frequency is scanned over a relative large range. The Rabi transition probability is logged versus the laser frequency. When the scanning range is more than 200 kHz, the sideband-resolved spectra are obtained, as shown in Fig. 2. The fitting of the sidebands shows that the temperature of the lattice trapped atoms is  $\sim 4 \mu\text{K}$  in the longitudinal axis and  $\sim 10 \mu\text{K}$  in the radial direction.<sup>[10]</sup>

After the second stage laser cooling, the atoms are optically pumped to  $|F = 9/2, m_F = +9/2\rangle$  and  $|F = 9/2, m_F = -9/2\rangle$  stretched states alternatively by using either  $\sigma^+$  or  $\sigma^-$  polarization of the 689 nm laser at  $^1S_0$  ( $F=9/2$ )– $^3P_1$  ( $F=9/2$ ) transition frequency and spin-polarized.<sup>[9]</sup> The 698 nm probe

\*Supported by the National Natural Science Foundation of China under Grant Nos 91336212 and 91436104.

\*\*Corresponding author. Email: linyige@nim.ac.cn

© 2015 Chinese Physical Society and IOP Publishing Ltd

laser is co-aligned with the lattice laser and their polarization is aligned with the bias magnetic field ( $\sim 56 \mu\text{T}$ ) to resolve the two stretched states. When atoms are optically pumped to a single spin sub-state, the Rabi transition linewidth is as narrow as 3 Hz for a 698-nm probe pulse width of 320 ms, as shown in the inset of Fig. 2. The actual lock utilizes 80 ms pulse width (the Fourier-limited Rabi linewidth is  $\sim 10$  Hz) to make it more reliable.

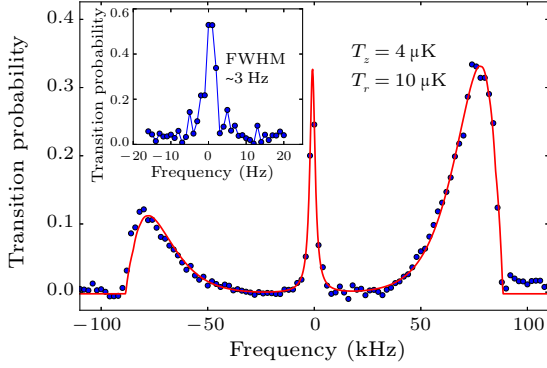


**Fig. 2.** Sideband resolved spectra of the  $^1S_0-^3P_0$  transition. The red line is the fitting of the experimental data, from which the atoms' temperature is derived. The inset is a high resolution spectrum (full width at half maximum  $\sim 3$  Hz) of a single Zeeman component of the  $^1S_0-^3P_0$  transition with a Rabi excitation pulse width of 320 ms.

**Table 1.** Frequency corrections and uncertainties of the strontium optical lattice clock and of the absolute frequency measurement in units of fractional frequency ( $10^{-16}$ ).

Contributor	Correction ( $10^{-16}$ )	Uncertainty ( $10^{-16}$ )
Lattice Stark	17.2	2.2
BBR Stark	49.7	0.7
2nd order Zeeman	1.8	0.1
Collision	12.0	0.3
Clock laser Stark	0	0.1
Line pulling	0	0.1
Sr total	80.7	2.3
Statistical		13
Gravitational	-50.6	1.1
Fountain calibration		31
Fiber transfer	0	<1
Measurement total		34

Figure 1(b) shows the locking schematic diagram of the clock laser to the atomic transition. A digital servo modulates the clock laser frequency alternatively to the two shoulders of a transition. The difference of the transition probabilities gives the frequency error of the clock laser with respect to the atomic transition. Two independent digital servos are used to lock the clock laser time-multiplexed to the two stretched state transitions. After 4 clock cycles, the average of the two digital lock frequencies gives the center frequency of the Sr clock transition.

Since we have only one optical clock, the systematic shifts were evaluated by the self-comparison approach.<sup>[11,12]</sup> Two independent atomic servos that share the same physical apparatus are compared in a

time-interleaved way. Only one parameter is modulated in a period of  $\sim 4$  s, which contains 4 clock cycles. Within this 4 s period, the clock laser is stable enough as the reference to compare the two atomic locked frequencies. The differential frequency between these two servos reflects the frequency shift induced by this modulated parameter. With this method, the systematic shifts were evaluated individually.

The top part of Table 1 lists the important systematic shifts of NIM's Sr optical lattice clock. The largest correction comes from the black-body radiation (BBR) induced shift. The BBR shift is<sup>[13]</sup>

$$\Delta\nu_{\text{BBR}} = \nu_{\text{static}} \left(\frac{T}{T_0}\right)^4 + \nu_{\text{dyn}} \left(\frac{T}{T_0}\right)^6, \quad (1)$$

where  $T$  is the ambient temperature seen by the atoms,  $T_0=300$  K,  $\nu_{\text{static}}$  is the BBR static coefficient, and  $\nu_{\text{dyn}}$  is the BBR dynamic coefficient. The higher order terms are negligible at the current uncertainty level. Here we cite  $\nu_{\text{static}} = -2.13023(6)$  Hz<sup>[14]</sup> and  $\nu_{\text{dyn}} = -0.1487(7)$  Hz.<sup>[3]</sup> The ambient temperature is recorded continuously during the experiments by three thin film PT100 sensing resistors. The ambient temperature  $22(1)^\circ\text{C}$  gives the BBR shift correction  $49.7(0.7) \times 10^{-16}$ .

The second dominating frequency shift and uncertainty come from the lattice ac Stark shift. Most reported optical lattice clocks use the special lattice wavelength called 'magic wavelength', where the first order ac Stark shift of the ground state and the excited state cancel each other.<sup>[15]</sup> To determine the magic wavelength, the frequency of the lattice laser needs to be changed in a wide range. In our case this is achieved by locking the lattice laser to different modes of its reference cavity. At one lattice frequency, the lattice trap depth is modulated between  $175E_r$  and  $109E_r$  alternatively,<sup>[16]</sup> where  $E_r$  is the lattice photon recoil energy. Due to the fact that the modulation of the lattice depth also changes the atomic cloud density, a correction according to the atomic number and the collision related coefficient (described later) is necessary. The dependence of the shift at  $I_0$  ( $I_0=162E_r$ ) to the lattice frequency is plotted in Fig. 3(a). The zero-shift frequency is determined to be  $368554672(44)$  MHz. During the absolute frequency measurements, the lattice laser frequency is locked to the nearest cavity mode, which is  $\sim 370(3)$  MHz away from the zero shift frequency and measured by the optical frequency comb. The lattice trap depth during the measurements is  $176(5)E_r$ . This gives the correction of  $17.2(2.2) \times 10^{-16}$ .

According to the Pauli exclusion principle, researchers usually believe that the collision between ultra cold fermionic  $^87\text{Sr}$  atoms would be completely suppressed. However, in practice the collisions could occur due to the inhomogeneous excitation.<sup>[11,17,18]</sup> The collisional shift is measured with the self-comparison method by alternating the atomic den-

sity. The density of the atoms trapped in the lattice is changed by applying different loading times from 200 ms to 800 ms in the first-stage laser cooling. The stability of a typical differential measurement is shown (red squares) in Fig. 4(a). Due to the higher atom number ( $\sim 10^4$ ) and relatively high atom temperature, we observed a larger density-dependent frequency shift. The calibration coefficient per volt of the photo-multiplier tube output is measured and plotted in Fig. 3(b). The atom number is recorded at every clock cycle while the clock is running, and this allows the point-to-point corrections of the density shifts to be performed. The correction for running the clock at high density is  $12.0(0.3) \times 10^{-16}$ .

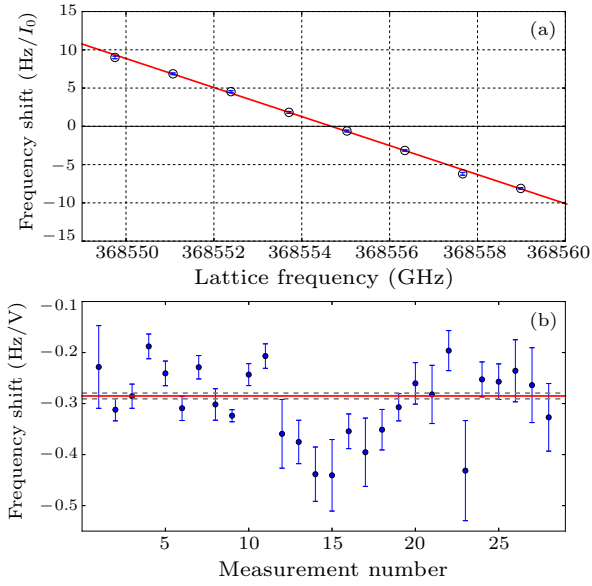


**Fig. 3.** (a) The dependence of the lattice ac stark shift at trap depth  $I_0$  ( $I_0 = 162E_r$ , where  $E_r$  is the recoil energy of the lattice photon) with respect to the lattice frequency. (b) The dependence of the collisional shift to the atom number. The atom number is represented by the fluorescence induced output voltage of the photomultiplier tube. The error bars show the statistical uncertainties of the measurements. The red solid line shows the weighted mean of the measurements and the dashed lines show the standard deviation of the combined statistical uncertainty.

The clock laser is alternatively locked to the  $m_F = +9/2$  and  $m_F = -9/2$  components of the clock transition at a small bias magnetic field. The average frequency of these two locks cancels the first order Zeeman shift, and the frequency difference between these two locks gives the real time estimation of the magnetic field at the atomic cloud position, which is used to evaluate the second order Zeeman shift. The coefficients of the first and second order Zeeman shifts have already been measured by some groups and have good agreements.<sup>[19–21]</sup> The frequency difference between these two locks is 556 Hz in our system and the second order Zeeman shift is estimated to be  $1.8(0.1) \times 10^{-16}$  with reference to the coefficient in Ref. [2].

The clock laser power is several nW and the Stark shift caused by the clock laser is very small (less

than  $0.1 \times 10^{-16}$ ) with reference to the coefficient in Ref. [22]. After the spin-polarization, the excitation of the atoms left in the other  $m_F$  states may cause the line shape asymmetric. With the transition linewidth of 10 Hz and the split between two adjacent  $m_F$  states of 62 Hz, less than 10% of atoms remain in the other states after spin-polarization contribute less than  $0.1 \times 10^{-16}$  uncertainty by line pulling effect. The dc Stark shift may occur when electric charges trapped on the MOT chamber fused silica viewports.<sup>[23]</sup> The charges can be removed effectively by shining UV light on the viewports.<sup>[23,24]</sup> A UV lamp is used to treat the viewports, and there is no significant shift found. Other effects, contributing very small shifts and uncertainties considering our present total uncertainty level, are omitted. The total systematic uncertainty of the Sr clock is  $2.3 \times 10^{-16}$ .

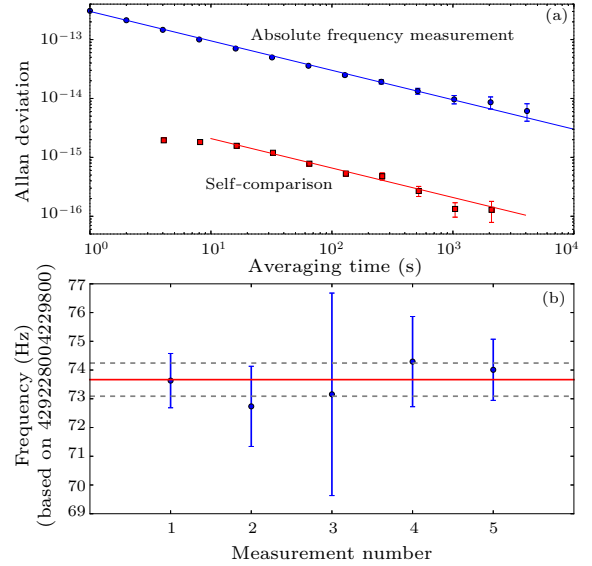


**Fig. 4.** (a) The measurement stability. The red solid squares show the Allan deviation (ADEV) of a typical self-comparison measurement of the collisional shift. The ADEV fits to (red line)  $6.6 \times 10^{-15} / \sqrt{\tau}$ . The blue circles show the ADEV of a typical absolute frequency measurement which fits to (blue line)  $3.0 \times 10^{-13} / \sqrt{\tau}$ . (b) The absolute frequency measurement results. The error bars show the statistical uncertainties of the measurements. The red solid line shows the weighted mean of the measurements and the dashed lines show the standard deviation of the combined statistical uncertainty.

The system setup for the absolute frequency measurement is shown in Fig. 5. The Sr lattice clock is located at NIM's Hepingli Campus, which is  $\sim 50$  km away from the NIM5 fountain and the H-maser in Changping Campus. A fiber link is established between the fountain lab and the Sr lab. Active FNC is applied to transfer the reference H-maser frequency to the Sr lab.<sup>[25]</sup> The FNC sender is referenced to the 100 MHz output from the H-maser, and up-converts the frequency to 9.2 GHz to modulate the 1.5  $\mu\text{m}$  laser transferred in the fiber. The FNC receiver down-converts the transferred frequency to 10 MHz. This signal is fed through a distribution amplifier to refer-

ence all the signal generators and frequency counters involved in the measurement. The Sr clock frequency is

$$f_{\text{Sr}} = N \cdot f_{\text{rep}} + f_0 + f_b - f_{\text{AOM3}} + f_{\text{AOM1}} + f_{\text{AOM2}}, \quad (2)$$

where  $f_{\text{rep}}$  is the comb repetition frequency,  $f_0$  is the comb offset frequency,  $f_b$  is the measured beat frequency between the atomic stabilized clock laser and the  $N$ th comb tooth,  $f_{\text{AOM1}}$  and  $f_{\text{AOM3}}$  are used to steer the clock laser frequency according to the atomic lock, and  $f_{\text{AOM2}}$  is 79 MHz of the FNC, which suppresses the noises in the fiber delivering the clock laser to the MOT. All the frequencies on the right side of Eq. (2) are referenced to the H-maser, which is calibrated by NIM5 throughout the measurement, thus the frequency of the Sr clock is traced to NIM5.

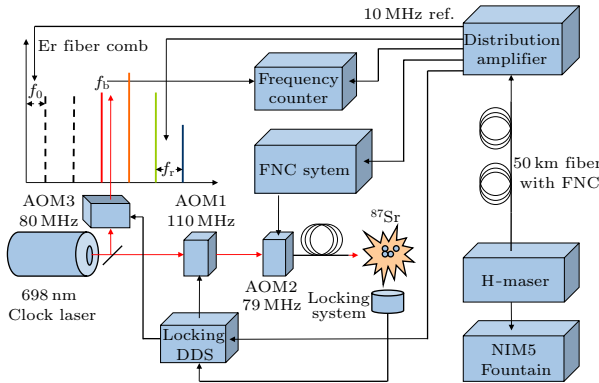


**Fig. 5.** The system setup for the absolute frequency measurement. AOM: acousto-optic modulator. FNC: fiber noise cancellation.

A total of 49113 s effective measurement data was acquired with 5 measurements, as shown in Fig. 4(b). The error bars in Fig. 4(b) show the statistical uncertainty of the measurements. According to Einstein's general theory of relativity, the gravitational shift needs to be considered when the clocks experience different gravitational potentials. The altitude of the atomic cloud measured by the large-scale dimensional metrology laboratory of NIM is 46.4(1.0) m, which is traced to a GPS receiver located on the roof of the lab building, and gives the shift  $50.6(1.1) \times 10^{-16}$ . The Allan deviation of one of the measurements is shown (blue circles) in Fig. 4(a). The statistical uncertainty of the total measurements is  $1.3 \times 10^{-15}$ . As listed in Table 1, the calibration uncertainty of NIM5 during the course of the measurements is  $3.1 \times 10^{-15}$ .

The uncertainty introduced by the fiber transfer system is less than  $1 \times 10^{-16}$ .<sup>[25]</sup> The absolute frequency of the Sr clock is 429228004229873.7(1.4) Hz. This result is consistent with the measurements carried out by other groups.<sup>[26–31]</sup>

In conclusion, we have built an optical lattice clock based on  $^{87}\text{Sr}$ . Its systematic uncertainty is evaluated to be  $2.3 \times 10^{-16}$ , which is mostly limited by the knowledge of the magic wavelength. The absolute frequency of the clock is traced to the NIM5 cesium fountain with an uncertainty of  $3.4 \times 10^{-15}$ , which is dominated by the uncertainty of the NIM5 fountain within the measurement periods of time limited by the Sr clock's running capability.

We would like to thank Zhang A. M., Gao Y. and Liang K. for fruitful discussions on the absolute frequency measurement, and Chen W. L. for the fiber transfer of the reference frequency.

## References

- [1] Chou C W et al 2010 *Phys. Rev. Lett.* **104** 070802
- [2] Bloom B J et al 2014 *Nature* **506** 71
- [3] Nicholson T L et al 2015 *Nat. Commun.* **6** 6896
- [4] Ushijima I et al 2015 *Nat. Photon.* **9** 185
- [5] Blatt S et al 2008 *Phys. Rev. Lett.* **100** 140801
- [6] Wang S K et al 2009 *Chin. Phys. Lett.* **26** 093202
- [7] Lin Y G et al 2013 *Chin. Phys. Lett.* **30** 014206
- [8] Li Y et al 2014 *Chin. Phys. Lett.* **31** 024207
- [9] Wang Q et al 2014 *Chin. Phys. Lett.* **31** 123201
- [10] Blatt S et al 2009 *Phys. Rev. A* **80** 052703
- [11] Swallows M D et al 2011 *Science* **331** 1043
- [12] Nicholson T L et al 2012 *Phys. Rev. Lett.* **109** 230801
- [13] Yudin V I et al 2011 *Phys. Rev. Lett.* **107** 030801
- [14] Middelmann T, Falke S, Lisdat C and Sterr U 2012 *Phys. Rev. Lett.* **109** 263004
- [15] Ido T and Katori H 2003 *Phys. Rev. Lett.* **91** 053001
- [16] Barber Z et al 2008 *Phys. Rev. Lett.* **100** 103002
- [17] Campbell G K et al 2009 *Science* **324** 360
- [18] Swallows M D et al 2010 *IEEE Trans. Ultrason. Ferroelectr. Freq. Control* **57** 574
- [19] Boyd M M et al 2006 *Science* **314** 1430
- [20] Falke S et al 2011 *Metrologia* **48** 399
- [21] Westergaard P G et al 2011 arXiv:1102.1797
- [22] Baillard X et al 2007 *Opt. Lett.* **32** 1812
- [23] Lodewyck J et al 2012 *IEEE Trans. Ultrason. Ferroelectr. Freq. Control* **59** 411
- [24] Pollack S E et al 2010 *Phys. Rev. D* **81** 021101
- [25] Wang B et al 2012 *Sci. Rep.* **2** 556
- [26] Campbell G K et al 2008 *Metrologia* **45** 539
- [27] Hong F L et al 2009 *Opt. Lett.* **34** 692
- [28] Yamaguchi A et al 2012 *Appl. Phys. Express* **5** 022701
- [29] Le Targat R et al 2013 *Nat. Commun.* **4** 2109
- [30] Falke S et al 2014 *New J. Phys.* **16** 073023
- [31] Akamatsu D et al 2014 *Appl. Phys. Express* **7** 012401



# Chinese Physics Letters

Volume 32

Number 9

September 2015

## GENERAL

- 090301 Quantum Illumination with Noiseless Linear Amplifier**  
ZHANG Sheng-Li, WANG-Kun, GUO Jian-Sheng, SHI Jian-Hong
- 090302 On Delay of the Delayed Choice Experiment**  
SUN Jun, SUN Yong-Nan, LI Chuan-Feng, GUO Guang-Can
- 090401 Seismic Noise Suppression for Ground-Based Investigation of an Inertial Sensor by Suspending the Electrode Cage**  
TAN Ding-Yin, YIN Hang, ZHOU Ze-Bing
- 090501 A Multifractal Detrended Fluctuation Analysis of the Ising Financial Markets Model with Small World Topology**  
ZHANG Ang-Hui, LI Xiao-Wen, SU Gui-Feng, ZHANG Yi
- 090601 First Evaluation and Frequency Measurement of the Strontium Optical Lattice Clock at NIM**  
LIN Yi-Ge, WANG Qiang, LI Ye, MENG Fei, LIN Bai-Ke, ZANG Er-Jun, SUN Zhen, FANG Fang, LI Tian-Chu, FANG Zhan-Jun
- 090701 Measurement of Refractive Index Ranging from 1.42847 to 2.48272 at 1064 nm Using a Quasi-Common-Path Laser Feedback System**  
XU Ling, TAN Yi-Dong, ZHANG Shu-Lian, SUN Li-Qun

## NUCLEAR PHYSICS

- 092501 Consistency of Perfect Fluidity and Jet Quenching in Semi-Quark-Gluon Monopole Plasmas**  
Jiechen Xu, Jinfeng Liao, Miklos Gyulassy

## ATOMIC AND MOLECULAR PHYSICS

- 093201 Dual-Wavelength Bad Cavity Laser as Potential Active Optical Frequency Standard**  
XU Zhi-Chao, PAN Duo, ZHUANG Wei, CHEN Jing-Biao
- 093401 Nucleus-Nucleus Effects in Fully Differential Cross Sections for Energetic  $C^{6+} + He$  Collisions with Small Momentum Transfer**  
LU Chen-Wen, AN Wen-Fang, SUN Shi-Yan, JIA Xiang-Fu

## FUNDAMENTAL AREAS OF PHENOMENOLOGY(INCLUDING APPLICATIONS)

- 094101 Giant Asymmetric Transmission and Optical Rotation of a Three-Dimensional Metamaterial**  
HUANG Lei, FAN Yun-Hui, WU Shan, YU Li-Zhi
- 094201 High-Power Continuous-Wave Nd:GdVO<sub>4</sub> Solid-State Laser Dual-End-Pumped at 880 nm**  
MAO Ye-Fei, ZHANG Heng-Li, SANG Si-Han, ZHANG Xin, YU Xi-Long, XING Ji-Chuan, XIN Jian-Guo, JIANG Yi
- 094202 Theoretical Study of Local Surface Plasmon Resonances on a Dielectric-Ag Core-Shell Nanosphere Using the Discrete-Dipole Approximation Method**  
MA Ye-Wan, WU Zhao-Wang, ZHANG Li-Hua, LIU Wan-Fang, ZHANG Jie
- 094203 Electromagnetically Induced Self-Imaging in Four-Level Doppler Broadening Medium**  
WANG Chun-Fang, WANG Feng, YANG Li-Ru
- 094204 A Polarization-Insensitive Broadband Metamaterial Absorber at the Optical Regime**  
SHI Jun-Xian, ZHANG Wen-Chao, XU Wan, ZHU Qing, JIANG Xia, LI Dong-Dong, YAN Chang-Chun, ZHANG Dao-Hua
- 094205 Electromagnetic Scattering of a High-Order Bessel Trigonometric Beam by Typical Particles**  
CUI Zhi-Wei, HAN Yi-Ping, CHEN An-Tao

JUST FOR AUTHORS  
— CHINESE PHYSICS LETTERS

- 094206 A Single-Frequency Linearly Polarized Fiber Laser Using a Newly Developed Heavily Tm<sup>3+</sup>-Doped Germanate Glass Fiber at 1.95 μm**  
 YANG Qi, XU Shan-Hui, LI Can, YANG Chang-Sheng, FENG Zhou-Ming, XIAO Yu, HUANG Xiang, YANG Zhong-Min
- 094207 A 60 W Tm:YLF Laser with Triple Tm:YLF Rods**  
 ZHU Guo-Li
- 094301 Vector Based Reconstruction Method in Magneto-Acousto-Electrical Tomography with Magnetic Induction**  
 GUO Liang, LIU Guang-Fu, YANG Yan-Ju, LIU Guo-Qiang
- 094302 Analysis of Long-Range Transmission Loss in the West Pacific Ocean**  
 WU Li-Li, PENG Zhao-Hui
- 094501 Self-Organized Criticality Theory Model of Thermal Sandpile**  
 PENG Xiao-Dong, QU Hong-Peng, XU Jian-Qiang, HAN Zui-Jiao

### PHYSICS OF GASES, PLASMAS, AND ELECTRIC DISCHARGES

- 095201 Characteristics of Resistance Triggering of a Pulsed Vacuum Arc Ion Source**  
 LAN Chao-Hui, LONG Ji-Dong, ZHENG Le, DONG Pan, YANG Zhen, WANG Tao, LI Jie
- 095202 How Does the Guide Field Affect the Asymmetry of Hall Magnetic and Electric Fields in Fast Magnetic Reconnection?**  
 LAI Xiang-Sheng, ZHOU Meng, DENG Xiao-Hua, LI Tang-Mu, HUANG Shi-Yong

### CONDENSED MATTER: STRUCTURE, MECHANICAL AND THERMAL PROPERTIES

- 096101 Fabrication of Amorphous Silver Nanowires by Helium Ion Beam Irradiation**  
 Shehla H., Ali A. Zongo S. Javed I. Ishaq A. Khizar H. Naseem S. Maaza M.
- 096102 Electronic and Optical Properties of TiS<sub>2</sub> Determined from Generalized Gradient Approximation Study**  
 Hamza El-Kouch, Larbi El Farh, Jamal Sayah, Allal Challioui
- 096201 Ultra-Hard Bonds in P-Carbon Stronger than Diamond**  
 GUO Wen-Feng, WANG Ling-Sheng, LI Zhi-Ping, XIA Mei-Rong, GAO Fa-Ming
- 096501 Low Thermal Conductivity of Paperclip-Shaped Graphene Superlattice Nanoribbons**  
 LU Xing, ZHONG Wei-Rong
- 096801 Nanoindentation Models of Monolayer Graphene and Graphyne under Point Load Pattern Studied by Molecular Dynamics**  
 XIANG Lang, WU Jian, MA Shuang-Ying, WANG Fang, ZHANG Kai-Wang

### CONDENSED MATTER: ELECTRONIC STRUCTURE, ELECTRICAL, MAGNETIC, AND OPTICAL PROPERTIES

- 097101 Effects of Si δ-Doping Condition and Growth Interruption on Electrical Properties of InP-Based High Electron Mobility Transistor Structures**  
 ZHOU Shu-Xing, QI Ming, AI Li-Kun, XU An-Huai, WANG Li-Dan, DING Peng, JIN Zhi
- 097102 Structural and Transport Properties of the Weyl Semimetal NbAs at High Pressure**  
 ZHANG Jun, LIU Feng-Liang, DONG Jin-Kui, XU Yang, LI Na-Na, YANG Wen-Ge, LI Shi-Yan
- 097401 A New Quantity to Characterize Stochastic Resonance**  
 WANG Yu-Xin, ZHAI Ji-Quan, XU Wei-Wei, SUN Guo-Zhu, WU Pei-Heng
- 097501 The Model for Linear Magnetoresistance of Two-Dimensional Metal-Semiconductor Composites with Interfacial Shells**  
 XU Jie, WANG Guo-Dong, LI Shan-Dong, LI Qiang, GAO Xiao-Yang
- 097701 Three-Dimensional Phase Field Simulations of Hysteresis and Butterfly Loops by the Finite Volume Method**  
 XI Li-Ying, CHEN Huan-Ming, ZHENG Fu, GAO Hua, TONG Yang, MA Zhi

- 097801 Top-Emitting White Organic Light-Emitting Diodes Based on Cu as Both Anode and Cathode**  
 MU Ye, ZHANG Zhen-Song, WANG Hong-Bo, QU Da-Long, WU Yu-Kun, YAN Ping-Rui, LI Chuan-Nan, ZHAO Yi
- 097802 Time-Resolved Photoluminescence Study of Silicon Nanoporous Pillar Array**  
 WANG Xiao-Bo, YAN Ling-Ling, LI Yong, LI Xin-Jian
- 097803 High-Efficiency Green Phosphorescent Organic Light-Emitting Diode Based on Simplified Device Structures**  
 ZHANG Hong-Mei, WANG Dan-Bei, ZENG Wen-Jin, YAN Min-Nan
- 097804 Effect of High-Temperature Annealing on Yellow and Blue Luminescence of Undoped GaN**  
 CHAI Xu-Zhao, ZHOU Dong, LIU Bin, XIE Zi-Li, HAN Ping, XIU Xiang-Qian, CHEN Peng, LU Hai, ZHANG Rong, ZHENG You-Dou

### CROSS-DISCIPLINARY PHYSICS AND RELATED AREAS OF SCIENCE AND TECHNOLOGY

- 098101 A Facile Route to Cotton-Like BiOCl Nanomaterial with Enhanced Dye-Sensitized Visible Light Photocatalytic Efficiency**  
 ZHAO Mei, DONG Li-Feng, LI Cheng-Dong, YU Li-Yan, LI Ping
- 098102 Morphological and Microstructural Evolution and Related Impurity Incorporation in Non-Polar  $a$ -Plane GaN Grown on r-Sapphire Substrates**  
 JIANG Ren-Yuan, XU Sheng-Rui, ZHANG Jin-Cheng, JIANG Teng, JIANG Hai-Qing, WANG Zhi-Zhe, FAN Yong-Xiang, HAO Yue
- 098103 Facile Synthesis of Rose-Like NiO Nanoparticles and Their Ethanol Gas-Sensing Property**  
 ZHANG Yong, XIE Long-Zhen, LI Hai-Rong, WANG Peng, LIU Su, PENG Ying-Quan, ZHANG Miao
- 098201 Quasiclassical-Trajectory Investigation on the Isotopic Effect of  $H(D)+LiF \rightarrow H(D)F+Li$  ( $v = 0-4, j = 0$ ) Reaction**  
 XIE Ting-Xian, ZHANG Ying-Ying, SHI Ying, JIN Ming-Xing
- 098501 Solution-Processed High Mobility Top-Gate N-Channel Polymer Field-Effect Transistors**  
 XIANG Lan-Yi, YING Jun, HAN Jin-Hua, WANG Wei, XIE Wen-Fa
- 098502 A Novel Interface-Gate Structure for SOI Power MOSFET to Reduce Specific On-Resistance**  
 HU Sheng-Dong, JIN Jing-Jing, CHEN Yin-Hui, JIANG Yu-Yu, CHENG Kun, ZHOU Jian-Lin, LIU Jiang-Tao, HUANG Rui, YAO Sheng-Jie
- 098503 Close-Loop Bell-Bloom Magnetometer with Amplitude Modulation**  
 HUANG Hai-Chao, DONG Hai-Feng, HAO Hui-Jie, HU Xu-Yang

JUST FOR AUTHORS  
 — CHINESE PHYSICS LETTERS